DFT-Based Characterization of the Multiple Adsorption Modes of Nitrogen Oxides on Pt(111)

ARTICLE *in* THE JOURNAL OF PHYSICAL CHEMISTRY C · DECEMBER 2006

Impact Factor: 4.77 · DOI: 10.1021/jp064841p

2 AUTHORS:

Rachel Getman
Clemson University
24 PUBLICATIONS **771** CITATIONS
SEE PROFILE

William F Schneider
University of Notre Dame
205 PUBLICATIONS **4,393** CITATIONS
SEE PROFILE

Article

DFT-Based Characterization of the Multiple Adsorption Modes of Nitrogen Oxides on Pt(111)

Rachel B. Getman, and William F. Schneider

J. Phys. Chem. C, **2007**, 111 (1), 389-397• DOI: 10.1021/jp064841p • Publication Date (Web): 10 December 2006

DFT-Based Characterization of the Multiple Adsorption Modes of Nitrogen Oxides on Pt(111)

Rachel B. Getman[†] and William F. Schneider*[,†,‡]

Department of Chemical and Biomolecular Engineering and Department of Chemistry and Biochemistry, University of Notre Dame, 182 Fitzpatrick Hall, Notre Dame, Indiana 46556

Received: July 28, 2006; In Final Form: September 28, 2006

Pt is the most common catalyst for NO oxidation to NO_2, a key reaction in NO_x remediation chemistry. In this work, density functional theory calculations and plane-wave supercell models are used to calculate the energies, charge distributions, and vibrational spectra of the stable and metastable states of adsorbed NO, NO_2, and NO_3 on Pt(111), the most likely active metal face for this catalytic oxidation. NO, NO_2, and NO_3 are all strong electron acceptors and bind to the Pt(111) surface via charge donation from the surface. NO and NO_2, in particular, exhibit a variety of adsorption geometries, the most favorable at low coverage being those that maximize surface−adsorbate charge transfer through binding to multiple surface Pt. At low coverage, the order of binding energies is NO > NO_3> NO_2, and the oxidation of adsorbed NO to NO_2 is endothermic by 0.78 eV. Higher surface coverages favor migration of NO and NO_2 to lower-coordination surface sites due to competition for metal d charge density. These changes in surface binding configurations, along with the general decrease in surface−adsorbate bond energies associated with higher surface coverages, both tend to energetically promote NO conversion to NO_2 and are important in describing this catalytic chemistry.

1. Introduction

The effective remediation of NO_x ($x = 1, 2$), generated as byproducts of combustion, is a major outstanding challenge in environmental catalysis.[1−4] The catalytic oxidation of NO (g) to NO_2 (g)

$$\mathrm{NO\ (g)} + \frac{1}{2}\mathrm{O_2\ (g)} \rightarrow \mathrm{NO_2\ (g)} \qquad (1)$$

is a common element of most NO_x removal strategies, including the NO_x storage and reduction catalyst and NO_x selective catalytic reduction.[3−5] Supported Pt is the most common NO oxidation catalyst, and the kinetics and mechanism of NO oxidation have been the subject of several experimental investigations.[6−19] Recent evidence indicates that the rate of NO oxidation per available surface Pt site increases with increasing Pt particle size,[19] suggesting the low index Pt faces to be most active for the catalysis. Further, oxidation activity is associated with high coverages of surface O, although very high coverages appear to inhibit activity.[19] Finally, the reaction is apparently kinetically inhibited by the product NO_2.[17,19]

The NO oxidation reaction provides an interesting contrast to the more familiar CO oxidation reaction. NO oxidation to NO_2 is much less exothermic than CO oxidation to CO_2 and is equilibrium limited over reaction conditions of practical interest. Further, NO forms a number of higher oxides, notably NO_2 and NO_3, that can conceivably compete with adsorbed NO and O for catalytic surface sites. Thus, the relevant surface structures and kinetics of NO oxidation are likely quite different than for CO oxidation. Several atomistically detailed models of the NO oxidation reaction based on density functional theory (DFT)-derived parameters for the reaction kinetics have been reported.[20−23] These models are successful in describing important features of the catalysis, such as the sensitivity of the reaction kinetics to surface coverage. They are somewhat limited in terms of the surface species and reaction steps considered, neglecting to capture, for instance, the inhibition of the reaction by product NO_2.

A necessary step in developing a more complete description of Pt-catalyzed NO oxidation is enumeration and description of the various surface species relevant to the catalysis. The surface science of NO on Pt(111) has long been of interest due to its potential relevance to NO reduction catalysis,[24,25] and NO_2 adsorption on Pt(111) has garnered much attention as a low-pressure route to accessing higher oxygen coverages than are possible by O_2 dissociation.[26,27] However, the relationship of the surface species and their interconversion to NO oxidation activity remains to be clarified. As a step in this direction, in this work, we use large supercell DFT simulations to characterize the stable and some metastable states of adsorbed N, O, NO, NO_2, and NO_3 on a Pt(111) surface. Charge density analysis is used to characterize the nature and extent of interactions between the adsorbates and the surface, calculated harmonic vibrational frequencies are used to correlate the adsorbates with experimental observation, and the adsorption energies of all species are compared. In the low coverage limit, all adsorbates are thermodynamically unstable with respect to adsorbed NO, reinforcing the critical role of local surface coverage in promoting the conversion of NO to NO_2 on the Pt(111) surface.

2. Computational Details

DFT calculations were performed using the periodic supercell plane-wave basis approach, as implemented in the Vasp[28] code. Electron cores were described with the projector augmented-wave (PAW)[29,30] method, and plane waves were included to an

* To whom correspondence should be addressed. Phone: (574) 631-8754. Fax: (574) 631-8366. E-mail: wschneider@nd.edu.
† Department of Chemical and Biomolecular Engineering.
‡ Department of Chemistry and Biochemistry.

10.1021/jp064841p CCC: $37.00
Published on Web 12/10/2006

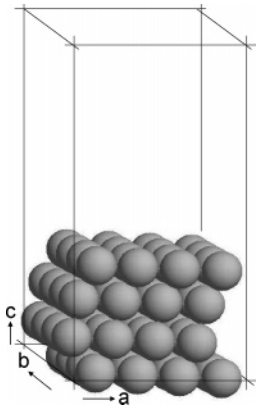

Figure 1. The four-layer thick 4 Pt × 4 Pt supercell.

energy cutoff of 400 eV. Electronic energies were computed with the PW91 implementation of the generalized gradient approximation (GGA).[31,32] Ionic relaxations were performed until the energy difference between subsequent steps was less than 0.0001 eV. A Gaussian smearing profile with a smearing parameter of 0.10 eV was imposed at the Fermi level, and energies were extrapolated to zero smearing. Smearing introduces finite temperature and, hence, an entropy contribution to the electronic energy; the maximum contribution observed here was for the clean Pt(111) surface, which was 0.010 eV/atom.

Gas-phase atoms and molecules were simulated in supercells 12 Å on a side, large enough to ensure negligible interactions between neighboring cells. Spin polarization was applied as appropriate, electronic states had integer occupancies, and in order to capture their asymmetric electronic ground states, the NO molecule and O atom were computed with no symmetry.

The structure of bulk Pt was calculated within a primitive face-centered cubic (fcc) cell using a 10 × 10 × 10 Monkhorst−Pack[33] **k**-point mesh, Γ-centered to yield 600 total **k**-points, of which 35 are symmetry unique. With this **k**-point mesh, energies are converged to within 1 meV per Pt atom. The lattice parameter was calculated to be 3.9861 Å, in excellent agreement with previous reports.[34] The calculated lattice parameter exceeds the experimental value by 0.063 Å,[35] or 2%, consistent with the general tendency of the GGA to overestimate internuclear distances.

Platinum(111) supercells were constructed of four layers of 4 Pt × 4 Pt surface planes (Figure 1) and separated from vertical images by six layers of vacuum space. The atoms in the bottom-most layer of the supercell were fixed in the calculated bulk locations, and the atoms in the remaining three layers were allowed to relax. Supercell calculations were performed nonspin-polarized, and energies were converged to within 0.03 meV per Pt atom with a 6 × 6 × 1 Monkhorst−Pack[33] **k**-point sampling of the first Brillouin zone. The atoms in the top-most and second layers of the bare slab relaxed inward from their bulk positions by approximately 0.06 and 0.07 Å, respectively, and the third layer atoms relaxed by 0.01 Å. The Pt(111) surface energy was computed to be 1.45 J m^{-2}, in excellent agreement with other models.[36] To compare with previous literature results, some calculations were performed with Pt(111) supercells constructed of four layers of 2 Pt × 2 Pt surface planes. Energies in these supercells were converged to within 0.6 meV/atom with a 10 × 10 × 1 Monkhorst−Pack[33] **k**-point sampling.

Following standard convention, adsorption energies are reported as positive numbers and are calculated here for single molecules adsorbed in a supercell; for example

$$\mathrm{NO\ (g)} + * \rightarrow \mathrm{NO}* \qquad (2)$$

In this notation, ∗ denotes an adsorption site, and NO* denotes surface-bound nitric oxide. The adsorption energy is sensitive to the number of metal layers included in the Pt(111) slab and to the lateral dimensions of the supercell, the latter of which determines the effective interadsorbate spacing. All of the adsorbates considered here interact repulsively, such that their adsorption energies decrease with increasing coverage. We report both 1/16 ML (4 × 4) and 1/4 ML (2 × 2) adsorption energies in Table 1. The adsorption energies for NO, NO_2, and NO_3 are, on average, 0.06 eV greater at 1/16 ML than at 1/4 ML. The number of metal layers used also affects the Pt−Pt interactions within the slab and thus indirectly affects adsorbate−substrate bonding. We observe that the adsorption energies exhibit even−odd oscillations that attenuate with the number of metal layers. This phenomenon has been noted previously[37,38] with respect to other adsorbate properties. We estimate the absolute adsorption energy to be systematically diminished by 0.06 eV in the four-layer slabs. Other sources of error, such as the finite plane-wave energy cutoff and the finite effective temperature at the Fermi level, are expected to be on the order of a few meV.

Two approaches were used to analyze the charge transfer accompanying chemisorption. The total density of states (DOS) was decomposed into atom-centered contributions, or atomic DOS, by integrating the charge around each atom within cutoff radii of 1.46, 0.74, and 0.82 Å for Pt, N, and O, respectively. The atomic DOS were also projected onto spherical harmonics over the entire span of states to provide total s, p, and d partial DOS on each atom. For each adsorbate, in-plane and out-of-plane p DOS were summed over each ion, generating valence molecular orbital DOS. In addition, a Bader[39] charge analysis was applied, taking advantage of a recent implementation of the Bader method for Vasp.[40] The Bader analysis partitions space into nonspherical atomic regions defined by local minima in the charge density. Atom charges are obtained by integrating the local charge density over the volume of each region. The Bader regions are disjoint and space filling and thus give a unique partitioning of charge. Because the regions are not spherical, however, they do not lend themselves to decomposition into angular contributions. The Bader and DOS methods were used in conjunction to complement each other. While the results differ numerically, qualitative trends are in agreement.

Vibrational frequencies were calculated by two-sided finite differences in the DFT gradients. All of the atoms in the admolecule and its immediate neighbor Pt were included in the finite differences and were perturbed by ± 0.01 Å. Diagonalization of the second-derivative matrix provides the harmonic vibrational frequencies and eigenmodes.

3. Results

3.1. Gas-Phase NO, NO_2, and NO_3. One defining characteristic of the NO, NO_2, and NO_3 molecules is that they are all odd-electron radicals with doublet ground states, so some care must be taken in describing their electronic structures within DFT. NO has a $^2\Pi$ ground state, and the single π^* electron can either be distributed between both components of the π^* level, preserving $C_{\infty v}$ symmetry, or it can be localized in one of the π^* components in a symmetry-broken calculation. The bond length is insensitive to this choice, but the symmetry-broken molecule is 0.03 eV lower in energy and is the reference used here. Consistent with experiment, NO_2 has C_{2v} symmetry and a spatially nondegenerate $^2A_1$ ground state. NO_3 is a highly reactive molecule in the gas phase and is not expected to be a significant homogeneous product of NO oxidation. However,

TABLE 1: Adsorption Energies (E_{ads}, in eV), Change in Local Pt Separation (Δ(Pt−Pt), in Å), Increase in Local Pt Height (Δ(Pt−surface), in Å), and Local Pt−adsorbate Vertical Separation (Δ(Pt−adsorbate), in Å) of NO, NO_2, NO_3, O, and N on Pt(111)

		E_{ads}				
species	geometry	1/16 ML	1/4 ML	Δ(Pt−Pt)	Δ(Pt−surface)	Δ(Pt−adsorbate)
NO	fcc	2.00	1.93	0.132	0.153	1.119
	hcp	1.86		0.078	0.136	1.251
	atop	1.59		N/A	0.286	1.939
NO_2	μ-N,O-nitrito	1.35	1.29	0.075	0.140(N)	1.881(N)
					0.102(O)	1.984(O)
	O,O′-nitrito	1.25		0.066	0.097	2.132
	nitro	1.24		N/A	0.208	2.036
NO_3	O,O′-nitrato	1.67	1.62	0.004	0.099	2.113
	nitrato	1.17		0.173	0.034	2.223
O	fcc	4.38	4.36	0.212	0.075	1.075
	hcp	3.98		0.164	0.142	1.109
N	fcc	4.89	4.81	0.185	0.131	0.898
	hcp	4.71		0.116	0.144	0.979
	bridge	4.00		0.199	0.169	1.123

TABLE 2: Bader Charges of Gas-Phase and Adsorbed NO, NO_2, NO_3, O, and N in e^- (O_s Denotes Surface-Bound O)

		Atomic Charges		
structure	charge	N	O_s	O
NO (g)	0.00	+1.10		−1.10
NO fcc	−0.50	+0.10		−0.60
NO hcp	−0.50	+0.10		−0.60
NO atop	−0.15	+1.10		−1.25
NO_2 (g)	0.00	+0.70		−0.35
μ-N,O-nitrito	−0.45	+0.40	−0.45	−0.40
O,O′-nitrito	−0.40	+0.70	−0.55	
nitro	−0.35	+0.60		−0.48
NO_3 (g)	0.00	+0.81		−0.27
O,O′-nitrato	−0.50	+1.00	−0.50	−0.50
nitrato	−0.70	+0.80		−0.50
O fcc	−0.80		−0.80	
O hcp	−0.75		−0.75	
N fcc	−0.75	−0.75		
N hcp	−0.75	−0.75		
N bridge	−0.65	−0.65		

NO_3 adsorbates could well be formed under strongly oxidizing conditions, and thus it is useful as a reference to consider the gas-phase structure. In agreement with experiment,[41−43] the GGA predicts NO_3 to exhibit D_{3h} symmetry and a $^2A_2'$ ground state. The calculated gas-phase structures are shown in Figures 2a, 5a, and 7a and, again as expected for the GGA, uniformly overestimate experimental bond lengths by approximately 0.03 Å.[43,44] Table 2 shows the calculated Bader atomic charges; the N−O bonds are uniformaly polarized toward O, with the largest charge separation for NO. Table 3 shows the calculated harmonic frequencies and their assignments, all of which are close to the experimentally observed values.

3.2. Adsorbates. *3.2.1. NO.* The close-packed Pt(111) surface offers a number of potential adsorption sites for a NO molecule, including 1-fold coordination atop a single Pt, 2-fold coordination at a bridge site, and 3-fold coordination at so-called fcc and hcp sites. While the earliest evidence suggested NO to bind at bridge sites at low coverage,[24,45] more recent evidence from NEXAFS,[46] STM,[47,48] LEED,[47,49] HREELS,[48] and RAIRS[49] all concur that NO prefers to adsorb in fcc 3-fold hollow sites at low coverage on Pt(111). Previous DFT results[20,25,50−55] also predict the 3-fold hollow fcc adsorption site to be most stable at low coverage. This agreement between simulation and experiment stands in contrast to the well-documented inconsistency between experiment and DFT for the preferred site of CO binding on Pt(111).[34]

We find NO to bond N-down and normal to the Pt surface at fcc sites, with an increase in the N−O bond length of 0.046 Å over the gas phase (Figure 2b). The GGA-calculated adsorption energies at 1/16 ML and 1/4 ML are 2.00 and 1.93 eV, respectively (Table 1). Previously reported values at 1/4 ML range from 1.75 to 2.10 eV.[50−54] These differences can largely be attributed to the use of more modest three-layer slabs in most earlier work, which, as noted above, can have a noticeable effect on absolute adsorption energies. For example, we calculate the adsorption energy of NO at 1/16 and 1/4 ML on three-layer Pt slabs to be 2.18 and 2.06 eV, in good agreement with other recent reports.[52,53] Differences in pseudopotentials and **k**-point

TABLE 3: Vibrational Frequencies of Gas-Phase and Adsorbed NO, NO_2, and NO_3 in cm^{-1}

	Asymmetric Stretch		Symmetric Stretch		In-Plane Bend		Out-of-Plane Bend	
structure	calcd	exptl	calcd	exptl	calcd	exptl	calcd	exptl
NO (g)	1899	1876[44]						
NO fcc	1502	1490[49]						
NO hcp	1529	1508[49]						
NO atop	1702	1715[49]						
NO_2 (g)	1666	1618[43]	1334	1320[43]	732	750[43]		
μ-N,O-nitrito	1541	1560[26]	978	1180[26]	759	795[26]		
O,O′-nitrito	1274		1146		793			
nitro	1497		1266	1270[27]	759	767[27]		
NO_3 (g)	1319	1492[41]	1086	1080[41]	531	360[41]	753	762[41]
O,O′-nitrato	1510		947		718		691	
	1034				667			
nitrato	1123		941		616		584	

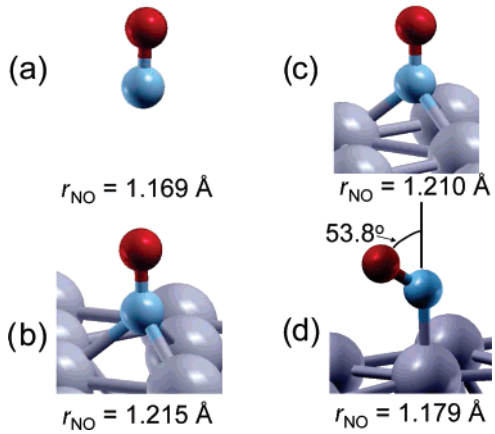

Figure 2. DFT-calculated gas-phase (a), fcc-bound (b), hcp-bound (c), and atop-bound (d) NO structures.

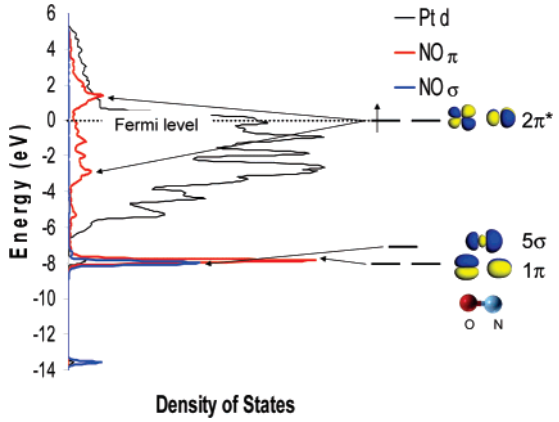

Figure 3. Orbital correlation diagram for fcc adsorption of NO on Pt(111). Right: Valence NO molecular states. Left: Contributions of NO σ (blue), π (red), and surface Pt d states to the total DOS.

sampling likely account for the balance of the discrepancies. We believe the methods applied here, including PAW potentials with well-converged **k**-point sampling and four-layer slabs, provide the best available DFT adsorption energy estimates.

Adsorption of NO, and in fact of all adsorbates considered in this work, causes the Pt atoms local to the adsorbate to relax laterally or parallel to the surface and away from the adsorbate, as well as vertically, or normal to, and upward from the surface. These relaxations can result in substantial changes in the Pt−Pt separations near the adsorbates. In Table 1, we report the lateral relaxation in terms of the increase in Pt−Pt separations of the atoms in the adsorption site relative to the Pt−Pt separation on clean Pt(111), and we report the vertical relaxation as the increase in height of these Pt molecules above the Pt surface atoms remote to the adsorption site. In the case of NO adsorption in a fcc site, for instance, the three Pt atoms nearest to N separate to a Pt−Pt distance of 2.95 Å, or 0.13 Å greater than on the clean Pt(111) surface, and vertically by 0.153 Å with respect to the Pt surface plane. The vertical distance between the three local Pt and N atoms is 1.119 Å. In general, the lateral Pt relaxations are smaller at higher surface coverage, and the Pt−adsorbate distances are greater. As surface coverage increases, more surface Pt becomes involved in the Pt−adsorbate bond, causing less pronounced vertical Pt relaxation.

Bader analysis (Table 2) indicates a net 0.50 electron transfer from Pt to the fcc-bound NO molecule. The origins of this charge transfer can be understood by reference to density of states (DOS) decompositions (Figure 3). Like CO,[56,57] NO has a filled 5σ donor state but, unlike CO, has one electron localized in the antibonding 2π* state. Because N is more electronegative than C, the NO 5σ and 2π* levels are lower in energy (by approximately 2 eV within the GGA) than are the corresponding CO levels. NO is thus an even stronger π acceptor than is CO,[58] and congruent with this, the GGA-calculated NO fcc adsorption energy is 0.13 eV greater than CO. The left side of Figure 3 shows the molecular NO valence orbitals and their mappings onto the surface Pt d DOS upon adsorption. The eigenvalues of both molecular and adsorbed NO are presented relative to the respective Fermi energy. Forward donation from the NO molecule 5σ level into Pt d levels stabilizes the 5σ orbital with respect to 1π and pushes some of the Pt d states above the Fermi level, resulting in weak σ bonding.[58,59] Most notably, however, is the strong mixing between the NO 2π* levels and the Pt d band that splits the 2π* into occupied Pt-bonding and unoccupied antibonding levels. In agreement with the Bader calculations, charge from the Pt surface flows into these 2π states, as reflected by a 0.30 electron increase in the integrated DOS π density from the gas phase to the surface. Occupation of this antibonding state lengthens the N−O bond, consistent with experimental observation based on NEXAFS.[46]

The calculated fcc NO stretch frequency is red-shifted 397 cm^{-1} relative to the gas phase (Table 3). Adsorbed NO vibrational spectra have been observed by HREELS[48] and RAIRS[49] and, due to the population of multiple adsorption sites, have a complicated behavior as a function of NO exposure. A band red-shifted 386 cm^{-1} relative to the gas phase has been assigned to fcc-bound NO, in good agreement with the results here.[48,49]

At high NO coverages, additional types of adsorption sites are reported to be populated on Pt[46−49,52] and other metals, such as Pd[60] and Rh.[61] We have characterized two other isomers of surface-bound NO, both of which are metastable at 1/16 ML coverage. The hcp isomer bonds N-down in a 3-fold hollow hcp site (Figure 2c). The bond length variations and charge distributions are quite similar to the fcc result, but the adsorption energy decreases by 0.14 to 1.86 eV, comparable to previous reports.[50,52] The calculated hcp vibrational frequency is red-shifted 370 cm^{-1} from gas-phase NO, slightly less than fcc NO and similar to the 368 cm^{-1} red shift for a NO vibrational mode assigned to hcp-bound NO at high NO exposures.[48,49]

In addition, NO can bind N-down and bent atop a single Pt (Figure 2d) at high NO coverages, as has been observed in a variety of experiments[45,46,48,49] and DFT calculations.[52,53,55] At 1/16 ML, we calculate the atop isomer to have a N−O bond length of 1.179 Å, an increase of 0.010 Å over the gas phase but significantly shorter than the 3-fold isomer bond lengths,[46] and to sit at an angle of 53.8° with respect to the surface normal. Adsorption causes the atop Pt to rise a rather large 0.29 Å above the surface plane. The atop adsorption energy is 1.60 eV at 1/16 ML coverage, 0.40 eV less than the fcc isomer. Consistent with this difference, the net charge transfer to atop NO obtained from the Bader charge analysis is only 0.15 electrons, and the charge distribution between N and O is quite similar to the gas-phase molecule. In line with this small charge transfer, the low-coverage atop NO vibrational frequency is calculated to be red-shifted only 197 cm^{-1} relative to the gas phase, consistent with the 161 cm^{-1} red shift reported experimentally.[48,49]

The stability of the atop isomer with respect to the fcc isomer increases with increasing surface coverage. At 1/2 ML of NO, calculated in a 2 Pt × 2 Pt supercell, we find the most stable configuration to have atop and fcc NO coadsorbed in equal proportions, as noted previously.[48,49,52] Similarly, in agreement with experiment,[45] we find coadsorption of O atoms to stabilize

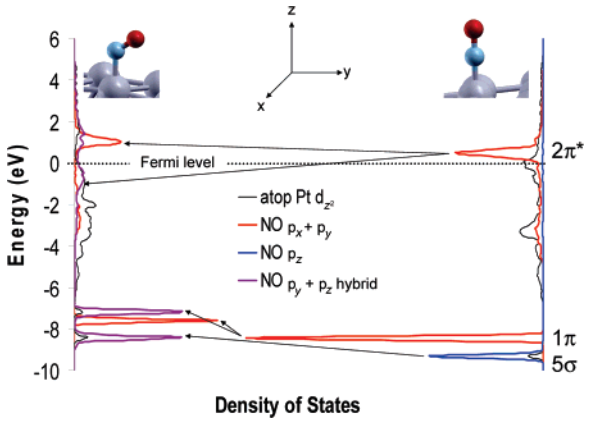

Figure 4. Orbital mixing associated with atop NO bending. Right: Contributions of NO σ (blue) and π (red) states and Pt d_{z^2} states to the total DOS of linearly adsorbed atop NO. Left: Contributions of NO σ (purple) and π (red) states and Pt d_{z^2} states to the total DOS of bent, atop NO.

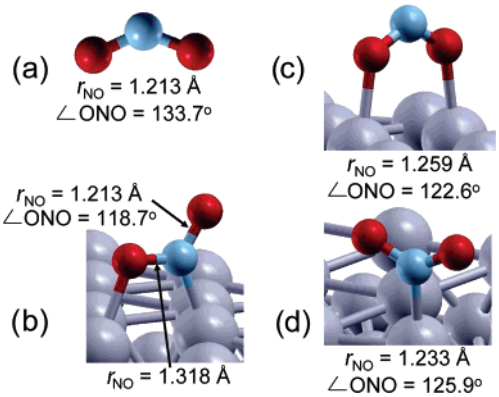

Figure 5. DFT-calculated NO_2 gas-phase (a), μ-N,O-nitrito (b), O,O′-nitrito (c), and nitro (d) isomers.

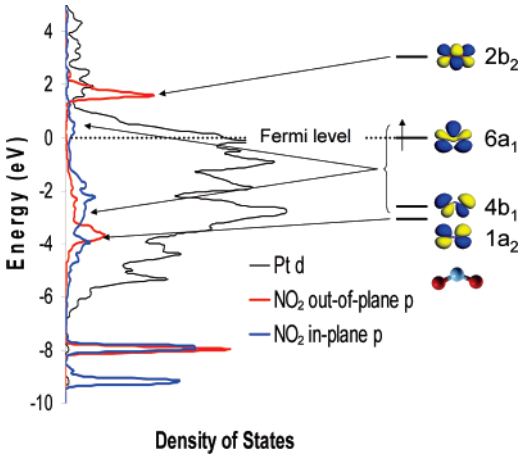

Figure 6. Orbital correlation diagram for μ-N,O-nitrito NO_2 adsorption on Pt(111). Right: Valence NO_2 molecular states. Left: Contributions of NO_2 in-plane (blue), out-of-plane (red), and surface Pt d states to the total DOS.

atop NO with respect to fcc NO; this preference for atop bonding at high O coverage could be significant in promoting the formation of NO_2 by reducing the NO motion necessary to form the new O−NO bond. By comparison, starting from fcc-bound NO and O, nudged elastic band calculations show that both adsorbates must migrate toward atop positions in order to form surface-bound NO_2.[20]

The much greater GGA-predicted preference for fcc over atop adsorption for NO (0.40 eV) than for CO (0.15 eV),[34] as well as the experimentally observed NO preference for fcc sites over atop, can both be traced to the π-acceptor strength of NO. On the basis of comparisons of the integrated DOS, π back-bonding from Pt to a NO constrained to adsorb atop and perpendicular to the Pt surface (Figure 4, right) is 0.8 electrons less effective than in a fcc site, due to poorer overlap between the $2\pi^*$ and Pt d states in the atop position. In order to compensate for the lack of donated Pt d density, atop NO bends with respect to the Pt surface, enhancing σ bonding at the expense of π bonding and increasing the binding energy by 0.5 eV. NO bending allows the 5σ and the partially filled in-plane $2\pi_y$ orbitals to hybridize into a N-centered lone pair and a half-filled orbital directed toward the atop Pt. The latter hybrid σ bonds effectively with the Pt d_{z^2} orbitals oriented normal to the Pt surface, as reflected in the enhanced mixing between the two shown on the left side of Figure 4. The π back-donation is weak and localized to the out-of-plane $2\pi_x$.[58,59] The strong π acceptor NO thus prefers fcc over atop sites at low coverage because of better π interactions with the surface in the former. When forced to compete with other adsorbates for Pt d density, as occurs at higher coverage, bent NO σ bonding at atop sites becomes more favorable. The weaker π-acceptor/better σ-donor CO discriminates less strongly between the two sites, and in fact, the GGA appears to reverse the actual atop over fcc site preference because it exaggerates the contributions of π back-bonding.[62,63]

3.2.2. NO_2. At low coverage, evidence from HREELS[26,27] and previously reported DFT calculations[20] indicates that NO_2 adsorbs onto Pt(111) with one N−O bond bridging two surface Pt atoms and the second N−O bond directed away from the surface, in the so-called μ-N,O-nitrito configuration. We find the same adsorption geometry here, shown in Figure 5b. Adsorption lengthens the surface-bound N−O bond by 0.105 Å while leaving the free N−O distance essentially unperturbed. Further, the O−N−O angle decreases by 15.0°. These modifications are consistent with those expected for a NO_2 strongly reduced by interaction with the surface. For instance, the O−N−O angle in ionic NO_2^- compounds is also approximately 15° less than that in free NO_2.[64] The GGA-calculated adsorption energy of μ-N,O-nitrito is 1.35 eV, or 0.65 eV less than NO. Adsorption causes modest restructuring of the Pt surface; the Pt atoms bound to the N and O atoms move apart by 0.08 Å and rise by 0.140 and 0.102 Å, respectively, relative to the Pt surface atoms not involved with the adsorbate−substrate bonds (Table 1).

As with fcc NO, Bader charge analysis indicates a substantial charge transfer from the Pt surface to adsorbed NO_2 (Table 2). The right side of Figure 6 shows the valence orbitals of molecular NO_2, which include filled nonbonding ($4b_1$) and half-filled antibonding ($6a_1$) orbitals of in-plane, or σ-like, symmetry, as well as lower-energy filled ($1a_2$) and higher-energy vacant ($2b_2$) orbitals of out-of-plane, or π, symmetry. The most significant bonding interactions occur between a hybridized combination of the in-plane NO_2 valence levels and the Pt d states. Integration of the in-plane NO_2 DOS indicates a charge transfer of 0.60 electrons from the Pt surface, and donation into the hybrid drives the lengthening of the N−O bond and opening of the O−N−O angle. In contrast, interactions with the out-of-plane NO_2 levels are more modest; the $2b_2$ level is pushed above the Fermi level and is essentially noninteracting with the Pt d states, while approximately 0.2 electrons flow from the $1a_2$ level to the Pt surface. Thus, as with NO, NO_2 bonding is dominated by donation from Pt to the adsorbate, but in-plane σ contributions greatly outweigh out-of-plane π ones.

We also located two metastable NO_2 isomers (Figure 5c,d), both of which have local C_{2v} symmetry and are of comparable energy and only about 0.10 eV less stable than the global minimum μ-N,O-nitrito isomer. In fact, the similarities in adsorption energies of the three isomers are quite striking, given their very different adsorption configurations. The O,O′-nitrito, or chelating, isomer adsorbs with both O atoms down and bridging two nearest-neighboring Pt atoms (Figure 5c). The N−O bonds are both lengthened by 0.046 Å, and the O−N−O angle is decreased by 11.1° relative to the gas-phase values, slightly less strongly perturbed than the μ-N,O-nitrito case. The bridged Pt atoms separate to a distance of 2.884 Å, notably larger than the O−O distance of 2.208 Å but similar to the Pt−Pt distance induced by μ-N,O-nitrito adsorption (Table 1). The Pt−O distances are over 2 Å, one of the longest adsorbate−substrate distances observed in this work. The Bader-calculated charge transfer to NO_2 is decreased by 0.05 electrons relative to that of μ-N,O-nitrito (Table 2). Bonding occurs primarily via Pt d donation into the half-filled, in-plane NO_2 $6a_1$ orbital, which has both the correct symmetry and orientation to interact with surface Pt orbitals; forward donation through the out-of-plane $1a_2$ level is negligible.

The least-strongly bound nitro isomer bonds N-down, planar, and atop Pt (Figure 5d). The N−O bonds are lengthened by 0.020 Å, and the O−N−O angle is decreased by 7.8°, both less strongly modified than in the μ-N,O-nitrito and O,O′-nitrito cases. Charge donation from Pt to NO_2 is weakest in the nitro isomer, as indicated by the Bader analysis (Table 2). Bonding again is primarily mediated through Pt d donation into the in-plane $4b_1$ and $6a_1$ NO_2 orbitals.

We have calculated the vibrational spectra of the three NO_2 isomers at a 1/16 ML coverage. The symmetric and asymmetric N−O stretch frequencies all red shift relative to the gas-phase values, in response to charge donation from the Pt surface (Table 3), while the O−N−O bending modes are less sensitive to adsorption. The two μ-N,O-nitrito N−O stretches decouple into a higher-frequency mode for the free N−O bond and into a much lower-frequency mode for the surface-bound N−O. In contrast, the splitting between the two stretch modes is diminished in the two C_{2v} isomers.

As with NO, the relative stabilities of these various NO_2 isomers are sensitive to surface coverage. Koel et al. have used vibrational HREELS to characterize these adsorption modes as a function of O coverage on Pt(111).[26,27] A mode observed at 1560 cm^{-1} has been attributed to the μ-N,O-nitrito isomer, and both the DFT adsorption energy and the vibrational frequency results support this assignment. A mode at 1180 cm^{-1} has been assigned to the second N−O stretch of this isomer, and here, the experiments and DFT results are in less satisfactory agreement. This discrepancy is possibly a consequence of differences in surface coverages between experiment and simulation, which could have a particularly large effect on vibrational motion parallel to the Pt surface. The observed band is also similar in energy to the calculated symmetric stretch of the C_{2v} O,O′-nitrito isomer, and an alternative possibility is that both isomers coexist under the conditions of experimental observation. A mode at 1270 cm^{-1} that appears with increasing O coverage has been assigned to the nitro isomer. The DFT results could be interpreted to support the assignment of this mode to either C_{2v} NO_2 isomer. In general, then, the DFT results are in agreement with the experimental evidence for the presence of more than one isomer of NO_2 under different coverage conditions, but further calculations that explicitly take into account the effects of O coverage are necessary to provide definitive assignments.

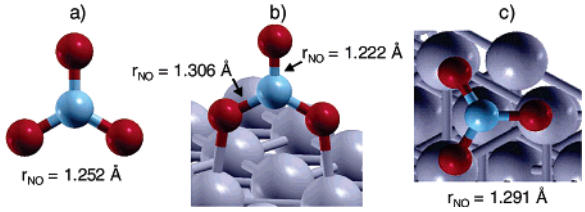

Figure 7. DFT-calculated gas-phase NO_3 (a), O,O′-nitrato (b), and nitrato (c) isomers.

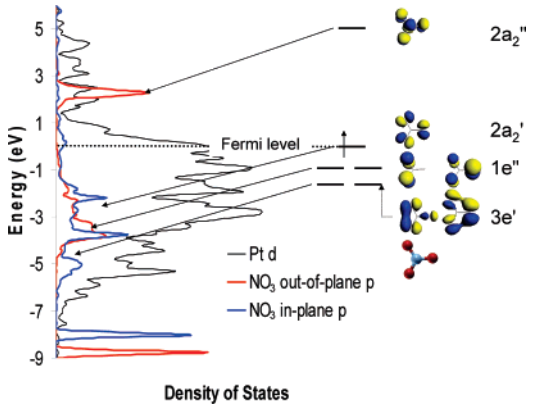

Figure 8. Orbital correlation diagram for O,O′-nitrato NO_3 adsorption on Pt(111). Right: Valence NO_3 molecular states. Left: Contributions of NO_3 in-plane (blue), out-of-plane (red), and surface Pt d states to the total DOS.

3.2.3. NO_3. To our knowledge, NO_3 adsorbates have not been explicitly identified on Pt(111). However, NO_3 adsorbates have been observed on Ag(110)[65] and Ag(111)[66−68] at high NO_2 exposures and have been suggested to account for some features in the temperature-programmed desorption of NO_2 from Pt(111) at high initial coverages.[26] DFT results indicate that NO_3 does bond to the Pt(111) surface. The most favorable configuration is similar in orientation to the O,O′-nitrito NO_2 isomer, including a trigonal-planar NO_3 adsorbate with two O atoms directed toward the surface and bridging two Pt atoms with local C_{2v} symmetry (Figure 7b). This configuration is labeled O,O′-nitrato. The bond distances between N and the two bridging O atoms increase by 0.054 Å from gas-phase NO_3 to 1.306 Å, while the terminal N−O bond is shortened by 0.030 Å. The NO_3 adsorbate is bound with respect to gas-phase NO_3 by 1.67 eV, intermediate between NO and NO_2. The Pt atoms separate negligibly in the lateral directions and rise 0.099 Å above the surface plane, and the Pt−O distances are 2.113 Å. The Pt−Pt and Pt−O distances are comparable to those of O,O′-nitrito (Table 1).

Bader decomposition indicates that 0.50 electrons transfer from Pt to NO_3 upon adsorption, comparable to the charge transfer found for NO and NO_2 adsorbates (Table 2). As shown on the right side of Figure 8, the NO_3 valence electronic structure is similar to NO_2 in having close lying filled and partially filled in-plane (3e′ and $2a'_2$) and filled and vacant out-of-plane (1e″ and $2a''_2$) levels. Also like NO_2, the primary orbital interactions upon adsorption involve mixing and charge transfer into the in-plane states from Pt d levels. Occupation of the in-plane levels increases by 0.4 electrons, while only 0.05 electrons are transferred to NO_3 through out-of-plane interactions.

O,O′-Nitrato adsorption causes the degenerate NO_3 asymmetric stretch to separate into higher- and lower-frequency modes (Table 3). The higher-frequency mode is similar to an

asymmetric stretching mode observed for a surface nitrate on Ag(111).[68] The symmetric stretch is red-shifted by 139 cm^{-1}.

Analogous to observations for NO_3 adsorption on basic metal oxides,[69] a metastable NO_3 adsorption mode can also be found in which the adsorbate binds planar and side-on to Pt(111) with local D_{3h} symmetry (Figure 7c). This nitrato adsorption energy is 1.17 eV, or 0.50 eV less than the perpendicular-bound O,O′-nitrato isomer. Here, charge transfer from the surface to the adsorbate is a substantial 0.70 electrons, and the distance between the surface and the adsorbate is more than 2.2 Å. The bonding thus has a large electrostatic component and is likely only important under conditions in which the Pt surface is electron rich.

3.2.4. O and N. In order to compare the energies of Pt-adsorbed NO, NO_2, and NO_3, it is useful to have their surface-bound atomic constituents, O and N, as energy references. Both O and N atoms are well-known to prefer fcc sites on Pt(111) at low coverages. The PW91-GGA binding energies referenced to gas-phase O(^{3}P) and N(^{4}S) are 4.38 and 4.89 eV, respectively (Table 1), in good agreement with previously reported results.[20,57,70,71] These binding energies decrease at 1/4 ML by 0.02 and 0.08 eV, respectively, an amount commensurate with that for the various molecular adsorbates. As shown by Bader analysis, at 1/16 ML, charge transfer to both atoms in these sites is substantial (Table 2), reflecting the large electronegativities of both atoms. Binding at hcp sites is found to be less favorable by 0.40 and 0.18 eV for O and N, respectively, in good agreement with previously reported results.[72] Bridge-bonded N is also metastable; in contrast, the bridge site is a transition state for O diffusion between hcp and fcc sites.[73]

Because of ambiguities in the definition of the atomic ground states within DFT,[74] it is both more convenient and, due to cancellation of overbinding errors between the metal−atom and atom−atom bonds, more accurate to report these atomic binding energies with respect to the calculated gas-phase O_2 and N_2 molecules.

$$\frac{1}{2}X_2\,(g) \rightarrow X^* \qquad (3)$$

On this basis, the 0 K binding energies are 1.29 and −0.28 eV for an O and a N atom, respectively. Note that N adsorbs endothermically with respect to N_2. While we are unaware of any experimental determination of the N binding energy, the O binding energy can be compared to the observed single-crystal heat of adsorption of O_2 on Pt(111) reported by King et al.[75] The adsorption heat was obtained by pulsing an O_2 molecular beam at a Pt(111) crystal surface and measuring both the temperature rise due to exothermic dissociative adsorption and the pressure rise due to molecular scattering and desorption. Extrapolating to low coverage and ignoring adsorption likely due to surface defects, the dissociative adsorption energy is reported to be 1.58 eV at 298.15 K. Correcting to 0 K using the tabulated heat capacities[76] and removing zero-point energy contributions using the DFT-calculated O−O zero-point energy decreases this to 1.46 eV. Using these estimates, the PW91-GGA underbinds O−Pt(111) by approximately 0.17 eV with respect to molecular O_2.

4. Discussion

As shown above, the likely intermediates in NO oxidation, including NO, NO_2, and NO_3, all adsorb exothermically on the Pt(111) surface, accompanied by substantial charge transfer from the surface to the adsorbates and modest surface relaxations. All three of these adsorbates have fairly large electron affinities

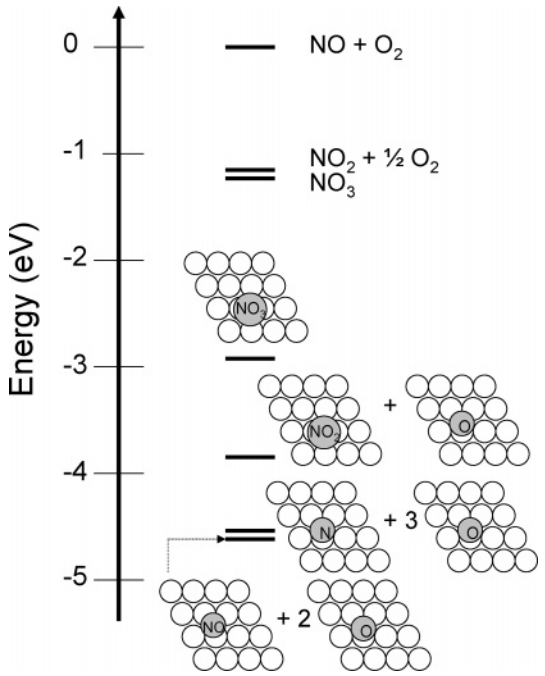

Figure 9. DFT-calculated energies of NO, NO_2, NO_3, and N at constant NO_3 stoichiometry at low coverage.

(0.026,[76] 2.273,[77] and 3.937 eV,[41] respectively) and either π (NO) or σ (NO_2, NO_3) orbitals available for accepting electron density. The observed structural changes and vibrational frequency shifts are consistent with those expected for reduced forms of the adsorbates. With respect to the gas-phase molecules, the order of binding energies is found to be NO > NO_3 > NO_2.

With respect to understanding the surface thermodynamics of NO oxidation, it is useful to consider the stabilities of the NO, NO_2, and NO_3 species relative to each other and to their atomic fragments. The relative DFT energies of the various adsorbate combinations at constant NO_3 stoichiometry and at 1/16 ML coverage of all species (i.e., approximately the low-coverage limit) are plotted in Figure 9. The most stable surface composition is dilute adsorbed NO and O, which is slightly lower in energy than atomic N and O and 0.78 eV lower in energy than adsorbed NO_2. Thus, consistent with previous evidence, the present DFT results show Pt(111)-adsorbed NO to be stable both to dissociation[25,51] as well as to oxidation to NO_2 via reaction with surface O in the absence of any lateral interaction effects.[20,26,27] Oxidation of adsorbed NO to adsorbed NO_3 is even more endothermic and, thus, energetically unfavorable at low surface coverage.

The DFT-calculated relative energies of gas-phase NO, NO_2, and NO_3 are also indicated on the same energy axis in Figure 9. The significant surface-adsorption energy of NO_2 likely accounts, at least in part, for the inhibiting effect of gaseous NO_2 on catalytic NO oxidation over Pt catalysts.[17,19] To the extent that catalytic NO oxidation does occur via a Langmuir−Hinshelwood-type mechanism on the Pt(111) surface, it is a result of modifications of the surface energetics arising from destabilizing lateral interactions between the adsorbates that promote both the conversion of NO to NO_2 and the desorption of NO_2.

Under practically relevant catalytic NO oxidation conditions, O_2 is present at partial pressures many orders of magnitude greater than NO, and thus, surface O is likely to be the dominant surface species. Clearly, by simple equilibrium arguments, higher O surface concentrations will tend to promote the formation of NO_2. Local configurational and lateral interaction

effects are of even greater importance, however. We have already noted that one significant effect of increasing surface coverage is to drive adsorbed NO and NO_2 to more weakly bound atop sites; the inherently larger destabilizing effect on NO compared to that on NO_2 will tend to have a promoting effect on the conversion of adsorbed NO to adsorbed NO_2. Conversion of surface-bound NO to NO_2 involves breaking of one surface Pt−O bond and formation of one O−NO. Higher O coverages favor this transformation in two ways, by weakening the Pt−O surface bond and by locally favoring a more compact single surface species (NO_2) over two species (NO and O). The magnitude of these effects must be on the order of 1 eV to reverse the low-coverage energetic preference for NO over NO_2. Previous DFT results[20,71] show that lateral interactions can be of this order of magnitude in the aggregate.

While the GGA energies reported here are the best available for the surface-bound nitrogen oxide species, the GGA does significantly overestimate the exothermicity of the gas-phase reactions of NO and O_2 to NO_2 (eq 1) and of NO_2 and O_2 to NO_3. At 0 K with zero-point contributions removed from the energies, the experimental NO oxidation energy is −0.64 eV compared to the GGA result of −1.18 eV. The energy for NO_2 oxidation to NO_3 is 0.45 eV (endothermic), while the GGA predicts it to be −0.07 eV (exothermic). As a consequence, the GGA significantly exaggerates the gas-phase equilibrium fractions of NO_2 and NO_3 over that of NO at any given condition. Further, unless fortuitously compensated for by errors in the GGA-calculated molecular adsorption energies, these overestimates also propagate to the surface reactions connecting NO to NO_2 and NO_2 to NO_3. The requirements for favorable surface catalysis, for instance in terms of the destabilizing lateral interactions induced by neighboring adsorbates, are even more stringent than those indicated by the GGA. Careful treatment of these effects will be important in any quantitative model of NO oxidation catalysis on Pt(111).

5. Conclusions

The DFT supercell results reported here illustrate the variety of nitrogen oxide adsorption states possible on the Pt(111) surface. At low coverage, adsorption is dominated by maximization of back-donation from the Pt surface to the strong electron acceptors NO, NO_2, and NO_3. These electronic effects are apparent in the calculated charge distributions and in perturbations of the surface and adsorbate density of states. NO in particular is strongly surface bound and is stable both to dissociation and to association with dilute surface O to form NO_2. These results are consistent with the well-known ability of NO_2 to act as an O-atom donor to the Pt(111) surface[26,27] and reflect the greater inherent strength of the Pt(111)−O bond than the O−NO one. NO_3 is relatively higher in energy and not likely to be stable in isolation on Pt(111).

NO and NO_2 are found to possess a number of metastable adsorption configurations at low coverage, in which they occupy lower-coordination adsorption sites and reorient with respect to the Pt surface. The lower stability of these configurations reflects less effective charge donation from the Pt surface to the adsorbate. At the higher surface coverages of NO_x and oxygen, relevant to catalytic oxidation conditions, competition for metal surface charge density will tend to favor these metastable configurations at the expense of the electron-withdrawing low-coverage configurations. In addition, lateral interactions between adsorbates weaken Pt(111)−O bonds and, thus, are important in shifting the surface energetics in favor of the formation of NO_2. Correct description of both the configurational and the energetic consequences of high surface coverages would appear to be important in capturing the energetics and kinetics of the interconversion of Pt-bound NO and NO_2. Examination of these effects is the topic of ongoing work.

Acknowledgment. We thank Dr. Ye Xu of Oak Ridge National Laboratory, Dr. Victor Ranea of the University of Notre Dame Radiation Laboratory, and Wenguang Lin of the University of Notre Dame Department of Chemistry and Biochemistry for their insights and assistance. This work was supported by the Department of Energy National Energy Technology Laboratory through the University Computational Materials Consortium. Some graphics were created using the XCrysDen (ref 78) software.

References and Notes

(1) Schneider, W. F. Fundamental Concepts in Molecular Simulation of NO_x Catalysis. In *Environmental Catalysis;* CRC Press: Boca Raton, FL, 2005; Chapter 10.
(2) Pârvulescu, V. I.; Grange, P.; Delmon, B. *Catal. Today* **1998**, *46*, 233.
(3) Shelef, M.; McCabe, R. W. *Catal. Today* **2000**, *62*, 35.
(4) Gandhi, H. S.; Graham, G. W.; McCabe, R. W. *J. Catal.* **2003**, *216*, 433.
(5) Epling, W. S.; Campbell, L. E.; Yezerets, A.; Currier, N. W.; Parks, J. E., II. *Catal. Rev.* **2004**, *46*, 163.
(6) Xue, E.; Seshan, K.; van Ommen, J. G.; Ross, J. R. H. *Appl. Catal., B* **1993**, *2*, 183.
(7) Xue, E.; Seshan, K.; Ross, J. R. H. *Appl. Catal., B* **1996**, *11*, 65.
(8) Burch, R.; Watling, T. C. *J. Catal.* **1997**, *169*, 45.
(9) Lee, J.-H.; Kung, H. H. *Catal. Lett.* **1998**, *51*, 1.
(10) Olsson, L.; Westerberg, B.; Persson, H.; Fridell, E.; Skoglundh, M.; Andersson, B. *J. Phys. Chem. B* **1999**, *103*, 10433.
(11) Oi-Uchisawa, J.; Obuchi, A.; Enomoto, R.; Liu, S.; Nanba, T.; Kushiyama, S. *Appl. Catal., B* **2000**, *26*, 17.
(12) Denton, P.; Giroir-Fendler, A.; Praliaud, H.; Primet, M. *J. Catal.* **2000**, *189*, 410.
(13) Corro, G.; Elizalde, M. P.; Velasco, A. *React. Kinet. Catal. Lett.* **2002**, *76*, 117.
(14) Marques, R.; Darcy, P.; Da Costa, P.; Mellottee, H.; Trichard, J.-M.; Djega-Mariadassou, G. *J. Mol. Catal. A: Chem.* **2004**, *221*, 127.
(15) Olsson, L.; Abul-Milh, M.; Karlsson, H.; Jobson, E.; Thormählen, P.; Hinz, A. *Top. Catal.* **2004**, *30/31*, 85.
(16) Crocoll, M.; Kureti, S.; Weisweiler, W. *J. Catal.* **2005**, *229*, 480.
(17) Mulla, S.; Chen, N.; Delgass, W. N.; Epling, W. S.; Ribeiro, F. H. *Catal. Lett.* **2005**, *100*, 267.
(18) Mulla, S. S.; Chen, N.; Cumaranatunge, L.; Blau, G. E.; Zemlyanov, D. Y.; Delgass, W. N.; Epling, W. S.; Ribeiro, F. H. *J. Catal.* **2006**, *241*, 389.
(19) Mulla, S. S.; Chen, N.; Cumaranatunge, L.; Delgass, W. N.; Epling, W. S.; Ribeiro, F. H. *Catal. Today* **2006**, *114*, 57.
(20) Ovesson, S.; Lundqvist, B. I.; Schneider, W. F.; Bogicevic, A. *Phys. Rev. B* **2005**, *71*, 115406.
(21) Neurock, M.; Wasileski, S. A.; Mei, D. *Chem. Eng. Sci.* **2004**, *59*, 4703.
(22) Kieken, L. D.; Neurock, M.; Mei, D. *J. Phys. Chem. B* **2005**, *109*, 2234.
(23) Mei, D.; Ge, Q.; Neurock, M.; Kieken, L.; Lerou, J. *Mol. Phys.* **2004**, *102*, 361.
(24) Gland, J. L.; Sexton, B. A. *Surf. Sci.* **1980**, *94*, 355.
(25) Brown, W. A.; King, D. A. *J. Phys. Chem. B* **2000**, *104*, 2578.
(26) Bartram, M. E.; Windham, R. G.; Koel, B. E. *Surf. Sci.* **1987**, *184*, 57.
(27) Bartram, M. E.; Windham, R. G.; Koel, B. E. *Langmuir* **1988**, *4*, 240.
(28) Kresse, G.; Fürthmuller, J. *Comput. Mater. Sci.* **1996**, *6*, 15.
(29) Blöchl, P. E. *Phys. Rev. B* **1994**, *50*, 17953.
(30) Kresse, G.; Joubert, D. *Phys. Rev. B* **1999**, *59*, 1758.
(31) Perdew, J. P.; Wang, Y. *Phys. Rev. B* **1992**, *45*, 13244.
(32) Perdew, J. P.; Chevary, J.; Vosko, S. H.; Jackson, K. A.; Pederson, M. R.; Singh, D. J.; Fiolhais, C. *Phys. Rev. B* **1992**, *46*, 6671.
(33) Monkhorst, H. J.; Pack, J. D. *Phys. Rev. B* **1976**, *13*, 5188.
(34) Feibelman, P. J.; Hammer, B.; Nørskov, J. K.; Wagner, F.; Scheffler, M.; Stumpf, R.; Watwe, R.; Dumesic, J. *J. Phys. Chem. B* **2001**, *105*, 4018.
(35) Wyckoff, R. W. G. *Crystallography Open Database;* http://www.crystallography.net/ (2006).
(36) Foiles, S. M.; Baskes, M. I.; Daw, M. S. *Phys. Rev. B* **1986**, *33*, 7983.

(37) Boisvert, G.; Lewis, L. J.; Scheffler, M. *Phys. Rev. B* **1998**, *57*, 1881.
(38) Bredow, T.; Giordano, L.; Cinquini, F.; Pacchioni, G. *Phys. Rev. B* **2004**, *70*, 035419.
(39) Bader, R. *Atoms in Molecules: A Quantum Theory;* Oxford University Press: New York, 1990.
(40) Henkelman, G.; Arnaldsson, A.; Jónsson, H. *Comput. Mater. Sci.* **2006**, *36*, 354.
(41) Weaver, A.; Arnold, D. W.; Bradforth, S. E.; Neumark, D. M. *J. Chem. Phys.* **1991**, *94*, 1740.
(42) Ishiwata, T.; Tanaka, I.; Kawaguchi, K.; Hirota, E. *J. Chem. Phys.* **1985**, *82*, 2196.
(43) Herzberg, G. *Molecular Spectra and Molecular Structure III. Electronic Spectra and Electronic Structure of Polyatomic Molecules;* Van Nostrand Reinhold: New York, 1966.
(44) Herzberg, G. *Molecular Spectra and Molecular Structure I. Spectra of Diatomic Molecules;* Van Nostrand Reinhold: New York, 1950.
(45) Bartram, M. E.; Koel, B. E.; Carter, E. A. *Surf. Sci.* **1989**, *219*, 467.
(46) Esch, F.; Greber, T.; Kennou, S.; Siokou, A.; Ladas, S.; Imbihl, R. *Catal. Lett.* **1996**, *38*, 165.
(47) Matsumoto, M.; Tatsumi, N.; Fukutani, K.; Okano, T.; Yamada, T.; Miyake, K.; Hate, K.; Shigekawa, H. *J. Vac. Sci. Technol., A* **1999**, *17*, 1577.
(48) Matsumoto, M.; Fukutani, K.; Okano, T.; Miyake, K.; Shigekawa, H.; Kato, H.; Okuyama, H.; Kawai, M. *Surf. Sci.* **2000**, *454*, 101.
(49) Matsumoto, M.; Tatsumi, N.; Fukutani, K.; Okano, T. *Surf. Sci.* **2002**, *513*, 485.
(50) Ford, D. C.; Xu, Y.; Mavrikakis, M. *Surf. Sci.* **2005**, *587*, 159.
(51) Liu, Z.-P.; Jenkins, S. J.; King, D. A. *J. Am. Chem. Soc.* **2003**, *125*, 14660.
(52) Aizawa, H.; Morikawa, Y.; Tsuneyuki, S.; Fukutani, K.; Ohno, T. *Surf. Sci.* **2002**, *514*, 394.
(53) Tang, H.; Trout, B. L. *J. Phys. Chem. B* **2005**, *109*, 17630.
(54) Ge, Q.; King, D. A. *Chem. Phys. Lett.* **1998**, *285*, 15.
(55) Burch, R.; Daniells, S. T.; Hu, P. *J. Chem. Phys.* **2002**, *117*, 2902.
(56) Blyholder, G. *J. Phys. Chem.* **1964**, *68*, 2772.
(57) Hammer, B.; Nørskov, J. K. *Adv. Catal.* **2000**, *45*, 71.
(58) Sung, S.-S.; Hoffmann, R.; Thiel, P. A. *J. Phys. Chem.* **1986**, *90*, 1380.
(59) Hoffmann, R. *Solids and Surfaces: A Chemist's View of Bonding in Extended Structures;* VCH Publishers: New York, 1988.
(60) Wickham, D. T.; Banse, B. A.; Koel, B. E. *Surf. Sci.* **1991**, *243*, 83.
(61) Wallace, W. T.; Cai, Y.; Chen, M. S.; Goodman, D. W. *J. Phys. Chem. B* **2006**, *110*, 6245.
(62) Kresse, G.; Gil, A.; Sautet, P. *Phys. Rev. B* **2003**, *68*, 073401.
(63) Mason, S. E.; Grinberg, I.; Rappe, A. M. *Phys. Rev. B* **2004**, *69*, 161401.
(64) Miletic, M.; Gland, J. L.; Hass, K. C.; Schneider, W. F. *J. Phys. Chem. B* **2003**, *107*, 157.
(65) Outka, D. A.; Madix, R. J.; Fisher, G. B.; Dimaggio, C. *Surf. Sci.* **1987**, *179*, 1.
(66) Brown, W. A.; Gardner, P.; King, D. A. *Surf. Sci.* **1995**, *330*, 41.
(67) Huang, W. X.; White, J. M. *Surf. Sci.* **2003**, *529*, 455.
(68) Alemozafar, A. R.; Madix, R. J. *Surf. Sci.* **2005**, *587*, 193.
(69) Schneider, W. F. *J. Phys. Chem. B* **2004**, *108*, 273.
(70) Bleakley, K.; Hu, P. *J. Am. Chem. Soc.* **1999**, *121*, 7644.
(71) Tang, H.; Van der Ven, A.; Trout, B. L. *Phys. Rev. B* **2004**, *70*, 045420.
(72) Feibelman, P. J.; Esch, S.; Michely, T. *Phys. Rev. Lett.* **1996**, *77*, 2257.
(73) Bogicevic, A.; Strömquist, J.; Lundqvist, B. I. *Phys. Rev. B* **1998**, *57*, R4289.
(74) Baerends, E. J.; Branchadell, V.; Sodupe, M. *Chem. Phys. Lett.* **1997**, *265*, 481.
(75) Yeo, Y. Y.; Vattuone, L.; King, D. A. *J. Chem. Phys.* **1997**, *106*, 392.
(76) NIST chemistry webbook, NIST standard reference database number 69. http://webbook.nist.gov/chemistry/ (2005).
(77) Ervin, K. M.; Hoe, J.; Lineberger, W. C. *J. Phys. Chem.* **1988**, *92*, 5405.
(78) Kokalj, Q. *J. Mol. Graphics Modell.* **1999**, *17*, 176.